Author Manuscript

Author Manuscript

Author Manuscript

Author Manuscript

HHS Public Access

Author manuscript

Neurobiol Aging. Author manuscript; available in PMC 2022 November 01.

Published in final edited form as:

Neurobiol Aging. 2021 November ; 107: 21–29. doi:10.1016/j.neurobiolaging.2021.07.006.

Dynactin 6 deficiency enhances aging-associated dystrophic neurite formation in mouse brains

Md Golam Sharoar[1,*], **John Zhou**[1,2], **Marc Benoit**[1], **Wanxia He**[1,2], **Riqiang Yan**[1]

[1]Department of Neuroscience, University of Connecticut Health, Farmington, CT., USA

[2]Molecular Medicine Graduate Program, Cleveland Clinic Lerner College of Medicine of Case Western Reserve University, Cleveland, OH., USA

Abstract

Formation of Reticulon 3 (RTN3)-immunoreactive dystrophic neurites (RIDNs) occurs early during the growth of amyloid plaques in Alzheimer's disease (AD) brains. We have shown that RIDNs in AD and aging mouse brains are composed of abnormally clustered tubular endoplasmic reticulum (ER) and degenerating mitochondria. To understand RTN3-mediated abnormal tubular ER clustering, we aimed to identify proteins that interact with RTN3 and impact accumulation of tubular ER in RIDNs. We found that the N-terminal domain of RTN3, which is unique among RTN family members, specifically interacted with dynactin 6 (DCTN6), a protein involved in dynein-mediated retrograde transport of cargo vesicles. DCTN6 protein levels decrease with aging in the hippocampal regions of WT mice. We found that DCTN6 deficiency enhanced RTN3 protein levels, high molecular weight RTN3 levels, and hippocampus-specific RIDN formation in aging brains of transgenic mice overexpressing RTN3. Our results suggest that the DCTN6-RTN3 interaction mediates tubular ER trafficking in axons, and a DCTN6 deficiency in the hippocampus impairs axonal ER trafficking, leading to abnormal ER accumulation and RIDN formation in brains of aging mice.

Keywords

Alzheimer's disease; Aging; dystrophic neurites; tubular ER; reticulon; RTN3; dynactin; DCTN6; axonal transport

[*]**Corresponding author**: Md Golam Sharoar, Ph.D., Department of Neuroscience, University of Connecticut Health, Farmington, CT 06030; Tel: 860-679-7132; sharoar@uchc.edu.

Author contribution

MGS deigned the experiment, performed most of the experiments, wrote this manuscript. JZ, MB and WH performed some experiments. RY mentored the experiment and critically edited this manuscript.

Conflict of interest

The authors declare no conflict of interest.

Publisher's Disclaimer: This is a PDF file of an unedited manuscript that has been accepted for publication. As a service to our customers we are providing this early version of the manuscript. The manuscript will undergo copyediting, typesetting, and review of the resulting proof before it is published in its final form. Please note that during the production process errors may be discovered which could affect the content, and all legal disclaimers that apply to the journal pertain.

Author Manuscript Author Manuscript Author Manuscript Author Manuscript

Introduction

The presence of dystrophic neurites (DNs) is one of distinguishing features in brains of Alzheimer's disease (AD) patients and a contributing factor to synaptic dysfunction (Hu et al., 2007; Joachim et al., 1989; Lenders et al., 1989). In AD brains, various proteins and organelles accumulate in DNs surrounding amyloid beta (Aβ) plaques (Dickson et al., 1999; Nixon et al., 2005; Sharoar et al., 2019). Reticulon 3 (RTN3), a tubular endoplasmic reticulum (ER)-shaping protein, was previously shown to mark an abundant population of DNs clustered around Aβ plaque in AD brains, and therefore named RTN3-immunoreactive DNs (RIDNs) (Hu et al., 2007; Shi et al., 2013).

Besides the clustered form of DNs surrounding Aβ plaques in AD brains, disperse RIDNs also emerge throughout the hippocampus CA1 region in aged wild-type (WT) mouse brains. Furthermore, the formation of disperse RIDNs is accelerated when RTN3 is overexpressed in transgenic RTN3 (Tg-RTN3) mouse brains (Hu et al., 2007; Shi et al., 2009). The presence of RIDNs impairs learning and memory in Tg-RTN3 mice, as determined by electrophysiological recordings and behavioral tests (Hu et al., 2007; Shi et al., 2013).

RTN3 is the neuronal-enriched member of the RTN family (with four members: RTN1 to RTN4), which is localized in the tubular domain of ER that controls the curvature of the ER membrane (Voeltz et al., 2006). All RTNs have a common C-terminal homology domain, known as an RTN homology domain (RHD), and a diversified N-terminal domain (Oertle and Schwab, 2003). Two transmembrane (TM) domains, TM1 and TM2, of RTNs are localized within the RHD and play critical roles in ER tubulation by membrane embedding via interaction with other ER tubule proteins such as the receptor expression-enhancing proteins (REEPs) (Sharoar et al., 2016; Sharoar and Yan, 2017; Voeltz et al., 2006). Interestingly, although RTN1 and RTN4 are also expressed by neurons, these two RTN family members are not enriched in RIDNs (Hu et al., 2007; Shi et al., 2017), suggesting no direct roles in the formation of DNs. RIDNs appear to interact with other tubular ER-shaping proteins, REEP2 and REEP5, in AD brains and in Tg-RTN3 mouse brains, and could have an age-dependent accumulation with tubular ER at axonal termini (Sharoar et al., 2016). Furthermore, RTN3-mediated tubular ER clustering also induces mitochondrial degeneration. Hence, RTN3 appears to be a key molecule for RIDN formation in aging mouse brains because REEP2/5-marked RIDNs are absent in older RTN3 knockout mouse brains (Sharoar et al., 2016).

Biochemically, RTN3 can form dimers and multimers, and high molecular weight (HMW)-RTN3 aggregates are often seen in the hippocampal area of brains (Hu et al., 2007; Shibata et al., 2008). The degree of HMW-RTN3 aggregate formation in Tg-RTN3 mouse hippocampi and in AD brains corresponds to the formation of dispersed and clustered RIDNs, respectively (Hu et al., 2007; Shi et al., 2009). In AD brains, Aβ-induced trafficking impairment and a defective proteasomal system have been suggested to stimulate the formation of HMW-RTN3 aggregates and clustered RIDNs surrounding Aβ plaques (Prior et al., 2010). However, how RTN3 aggregation and RIDN formation specifically occurs in the hippocampal region during aging in mouse brains is not yet clear.

Author Manuscript Author Manuscript Author Manuscript Author Manuscript

By utilizing yeast two-hybrid screening, we identified a subunit of dynein transport machinery complex, dynactin 6 (DCTN6), that interacts with the N-terminal domain of RTN3. We found that DCTN6 protein levels were reduced during aging in the hippocampus compared to the cortex in WT mouse brains. Knocking down DCTN6 enhanced RTN3 protein levels and the spontaneous formation of dispersed RIDNs in mouse brains. Although AAV-mediated overexpression of DCTN6 failed to attenuate RIDN formation in mouse brains, we found that DCTN6-RTN3 interactions altered tubular ER trafficking in axons. DCTN6 deficiency in the hippocampus impaired axonal transport of RTN3, and this impairment aggravated RTN3 aggregation, tubular ER accumulation, and RIDN formation in the aging mouse brain. Hence, DCTN6 appears to a regulator of RTN3 axonal transport, and worth further investigation to uncover its physiological functions.

Materials and Methods

Mouse strains

Tg-RTN3 mice were generated and genotyping was performed as described previously (Hu et al., 2007). DCTN6 heterozygous mutant mice (DCTN6+/−) were purchased from Jackson Laboratory (stock # 029000) and the genotyping was performed according to vendor instructions. Both Tg-RTN3 and DCTN6+/− strains were maintained by breeding with B6 mice (Jackson Lab stock # 000664). All mice in the study were maintained and used according to protocols approved by the Institutional Animal Care and Use Committee of the University of Connecticut.

Adeno-associated virus (AAV) particles

Custom-made AAV-syn-DCTN6-GFP (3.9×10^{13} GC/ml), AAV-syn-GFP (2.5×10^{13} GC/ml), and AAV-syn-RTN3 (1.5×10^{13} GC/ml) were purchased from Vector Biolabs (Malvern, PA). The viral particles were used according to protocols approved by the Institutional Biosafety Committee of the University of Connecticut.

Yeast Two-Hybrid (Y2H) Screening

Matchmaker Gold Y2H system containing pGADT7 and pGBKT7 vectors was purchased from Clontech (Mountain View, CA; Cat# 630489). First, the system was tested by mating positive (pGBKT7–53) and negative (pGBKT7-Lam) control vectors (bait) transformed Y2HGold strain and pGADT7-T vector (prey) transformed strain Y187. The mated cultures were grown on nutrient-deficient agar plates according to the manufacturer's protocol. Next, DNA encoding N-terminal (aa 1–61 and aa 7–61) and C-terminal regions of RTN3 were cloned into *EcoRI* and *BamHI* sites in the pGBKT7 vector. The autoactivation and toxicity of bait clones were tested by mating pGBKT7-RTN3 and pGBKT7 transformed Y2HGold strain with pGADT7-T vector (prey) transformed strain Y187. Then the pGBKT7-RTN3 transformed Y2HGold strain was mated with a Mate & Plate human brain cDNA library (Clontech; Cat# 603486), which contain ~1 million clones. The transformed strain was then grown on nutrient-deficient agar plates for 3–5 days at 30°C. The positive colonies were grown on double nutrient-deficient plates to remove any false positives. The positive colonies were picked and DNA was isolated, PCR amplified, and sequenced using a T7 promoter primer.

Author Manuscript Author Manuscript Author Manuscript Author Manuscript

Cell line and primary neuron culture

HEK293 cells were cultured in Dulbecco's Modified Eagle's Medium (DMEM; high glucose) and supplemented with 10% (v/v) fetal bovine serum (FBS) and 1% antibiotics at 37°C under 5% CO_2. The primary neurons from cortices and hippocampi of embryonic stage 18 (E18) WT or DCTN+/+ and DCTN6+/− mice were cultured separately in Neurobasal A medium (Gibco-Invitrogen) supplemented with B-27 (Gibco-Invitrogen) and 2 mM l-glutamine (Gibco-Invitrogen). Cultures were maintained at 37°C in a humidified atmosphere of 5% CO_2 and 95% air, fed twice a week, and maintained at least 7 days before the experiment.

Immunoprecipitation

For immunoprecipitation experiments with Tg-RTN3 mice brain extracts, snap-frozen brain sections were homogenized on ice in 1% CHAPS extraction buffer containing complete protease inhibitors (Roche Bioscience) and 0.1 mM Na_3VO_4 for inhibiting phosphatase. The homogenates were rotated for 30 min at 4 °C to ensure extraction of membrane proteins. After centrifugation at 15,000 × *g* for 120 min, supernatants were collected and protein concentrations were measured with bicinchoninic acid protein assay reagent (Thermo Scientific, Grand Island, NY, USA). Immunoprecipitation with transfected cell lysate was performed as described previously (Sharoar et al., 2016). In brief, HEK293 cells were first grown in DMEM for 24 hours in 60 mm plates to ~80% confluence and then transfected with the indicated expression constructs. After culturing for 48 hours, cells were lysed, and equal amounts of lysates (500 μg in 1 ml) were used for immunoprecipitation with Myc- or Flag-conjugated beads overnight. The extensively washed immunoprecipitants were resolved on a 4–12% NuPage Bis-Tris gel (Invitrogen) for Western blot assays.

Western blotting

Snap-frozen mouse brain cortices were homogenized on ice in RIPA buffer containing complete protease inhibitors (Roche Bioscience). The homogenates were rotated for 30 min at 4°C to ensure extraction of membrane proteins. After centrifugation at 15,000 x g for 120 min, supernatants were collected and protein concentrations were measured with bicinchoninic acid protein assay reagent (Thermo Scientific, Grand Island, NY, USA). Equal amounts of protein samples were resolved on 4–12% NuPage Bis-Tris gels (Invitrogen). Following incubation with the indicated primary antibody, an anti-rabbit or anti-mouse horseradish peroxidase-conjugated secondary antibody was added. Immunoreactivity was detected by chemiluminescence using Super Signal West PICO reagent (Thermo Scientific).

Immunofluorescent confocal microscopy

A standard method of immuno-confocal microscopy was performed as previously described (Hu et al., 2007). Briefly, mouse brains were dissected and fixed with 4% paraformaldehyde for 12 hours and immersed in 20% sucrose overnight at 4°C. The fixed brain tissue was then sectioned in the sagittal plane at a 14 μm thickness using a cryostat after O.C.T. compound embedding. Brain sections were stored at −20°C. After three washes with phosphate-buffered saline (PBS), the sections were permeabilized with 0.3% Triton X-100 for 30 min and rinsed in PBS three times to remove detergent. Antigen retrieval was

Author Manuscript Author Manuscript Author Manuscript Author Manuscript

then performed by heating in a microwave in 0.05 M citrate-buffered saline, pH 6.0, for 5 min. The sections were then blocked with 5% normal goat serum and incubated with individual primary antibodies: 6E10 (Covance Research Products, Inc; Cat# SIG-39330–200, RRID: AB_662804), β-Actin (Sigma Aldrich; Cat# A2228, RRID:AB_476697), Arp11 (Proteintech; Cat# 20101–1-AP, RRID:AB_10640424), calnexin (Sigma Aldrich; Cat# C4731, RRID:AB476845), c-Myc (Santa Cruz; Cat# sc-40, RRID:AB_2857941), DCTN4 (Thermo; Cat# MA5–17065, RRID:AB_2538536), DCTN5 (Abcam Cat# ab157197), DCTN6 (Proteintech; Cat# 16947–1-AP, RRID:AB_2245654), DCTN6 (Abcam Cat# ab197913), Flag (Sigma; Cat# F1804, RRID:AB_262044), MAP2 (Sigma; Cat# M4403, RRID:AB_477193), GFP (Roche; Cat# 1814460), m-Cherry (Cell Signaling; Cat# 43590), R458 polyclonal and RTN3 monoclonal (developed in the Yan lab), REEP2 (Proteintech; Cat# 15684–1-AP, RRID:AB_2238326), and Xpress (Invitrogen; Cat# 46–0528). After overnight incubation at 4°C, sections were washed with PBS three times and incubated with secondary antibodies conjugated with Alexa Fluor 488, Alexa Fluor 568, or Alexa Fluor 633 (Molecular Probes) for 2 hours at room temperature. The sections were finally washed with PBS 3 times and mounted with Vectasheild mounting medium. Sections were examined and images were captured with a Keyence bz-x710 fluorescence and Ziess LSM800 confocal microscope.

AAV injection into mouse brains

AAV-syn-mCherry, AAV-syn-RTN3-mCherry, AAV-syn-GFP, and AAV-syn-DCTN6-GFP were delivered to the left hippocampal region via a stereotaxic apparatus (Stoelting). After deep anesthesia via ketamine/xylazine and isoflurane inhalation, the mouse scalp was shaved and scrubbed with betadine, and 25 μl of 20% buprenorphine was injected intraperitonially before incision. The skull was exposed, and a 1.5 mm deep hole was drilled at a hippocampal region according to the atlas of Paxinos and Watson. With a 10 μl Hamilton syringe (model #1701), 5 μl of virus (8×10^{10} viral particles) for each group was injected into the brain at a rate of 0.5 μl/minute. Dental ceramic compound was applied over the drilling, and skin was attached with cyanoacrylate adhesive. After surgery, the same dose of buprenorphine was injected, and the mice were placed on a heating pad until fully awake and ambulatory. The mice were then placed in the animal facility room.

Image quantification and statistical analysis

Fiji (ImageJ) software was used to quantify the numbers and integrated density (Schindelin et al., 2012). The images were converted to 8-bit gray images and a fixed threshold was used to visualize the RIDN puncta or amyloid plaques. The numbers of RIDNs were counted in the hippocampus area/injected site on each image. To measure the size of RIDNs, the scale bar was first set and the area of each RIDN was measured. For quantification of Western blot images, the mean gray value for a fixed area was measured. Unpaired T-test of means was used to determine statistical significance, with p-value < 0.05 considered significant.

Author Manuscript Author Manuscript Author Manuscript Author Manuscript

Results

DCTN6 interacts with the N-terminal domain of RTN3

To understand how RTN3 mediates RIDN formation in the hippocampus, we speculated that an RTN3-interacting protein in the hippocampus facilitates this formation. We utilized a wellestablished yeast two-hybrid system to screen for RTN3-interacting partners in a human brain cDNA library that contains ~1 million clones. Our screen using N-terminal residues (amino acids 1–61) of the RTN3 protein as bait identified ~300 positive clones, and these were PCR amplified. Among the 300 clones, we obtained amplified DNA from only 41 clones, which were sequenced (supplemental Table 1). Translation of nucleotides sequenced from 41 clones and BLAST searching identified five matches with sequences encoding various lengths of DCTN6, which was further confirmed using a second bait spanning residues 8–61 of RTN3 (supplemental Table 1 and 2).

To validate this interaction, we performed co-immunoprecipitation (co-IP) using brain lysates from RTN3-myc-overexpressing transgenic (Tg-RTN3; myc-tagged) mice (Hu et al., 2007). Myc antibody effectively pulled down myc-tagged RTN3, and endogenous DCTN6 was co-IPed with RTN3 (Figure 1A). When endogenous DCTN6 was immunoprecipitated using a DCTN6-specific anybody, RTN3 was co-IPed (Figure 1B).

To further confirm the specific DCTN6-RTN3 interactions, we conducted a mapping study using various RTN3 truncation mutant constructs (He et al., 2006). HEK293 cells were co-transfected with Flag-tagged DCTN6 and Xpress-tagged RTN3 mutants, and cell lysates were used for co-IP experiments. We show that N-terminally deleted RTN3 (R3-ΔN61) failed to interact with DCTN6 (Figure 1D). Furthermore, full-length DCTN6 did not interact with RTN1, RTN2, or RTN4 (supplemental Figure 1), supporting the specific interaction between RTN3 and DCTN6. The RTN3-DCTN6 interaction in neurons was examined by co-localization of endogenous RTN3 and DCTN6 in primary neurons cultured from day 17 embryos (E17) of WT mouse brains using immuno-confocal microscopy. RTN3 was distributed in neuronal soma and neurites, and DCTN6 partially overlapped with RTN3 along neurites (Figure 1C). Quantification of RTN3 and DCTN6 colocalization among 5 randomly selected neurons showed an intensity correlation quotient (ICQ) coefficient of 0.32± 0.031 (Figure 1C, right panel). These results confirmed the specific interaction between DCTN6 and RTN3 via the N-terminal domain of RTN3.

DCTN6 deficiency enhances RTN3 protein levels and induces hippocampus-specific RIDN formation in wild-type aging mouse brains

RTN3 protein level increases during aging in the mouse brain, which correlates with the age-dependent formation of dispersed RIDNs in the hippocampus (Shi et al., 2009). Dispersed RIDN formation is accelerated in Tg-RTN3 mouse brains, due to overexpression of neuronal RTN3, and is correlated with synaptic dysfunction in those mice (Hu et al., 2007), resulting from abnormally accumulated tubular ER in the axonal terminus (Sharoar et al., 2016). Overexpression of GFP-tagged RTN3 in primary neurons cultured from the hippocampus is sufficient to induce an accumulation of tubular ER in the axonal boutons (Sharoar et al., 2016). The accumulation of such RTN3-GFP aggregates at the axonal bouton

Author Manuscript Author Manuscript Author Manuscript Author Manuscript

appeared more prominently in hippocampal neurons compared to those cultured from cortex (supplemental Figure 2a). We observed reduced DCTN6 protein levels in hippocampal regions, but enhanced DCTN4 protein levels in older mouse brains compared to younger mice (supplemental Figure 2b-d).

To investigate whether a reduced DCTN6 protein level in the hippocampus contributes to RIDN formation, we utilized DCTN6-deficient mice and investigated RIDN formation in DCTN6-deficient and Tg-RTN3 mouse brains. A DCTN6 heterozygous (DCTN6+/−) mouse was purchased from Jackson laboratory (stock # 029000; which was generated in Jackson Lab's random gene mutation projects). While DCTN6 homozygous mice were embryonic lethal, 6-month-old DCTN6+/− mice showed 40–25% reduction in DCTN6 protein levels in cortices and hippocampi compared to DCTN6+/+ mice (Figure 2A-B). DCTN6+/− mice also showed a reduction in DCTN5 protein levels, which was expected because DCTN6 and DCTN5 form a heterodimer and DCTN5 is unstable in the absence of DCTN6 (Yeh et al., 2012). Interestingly, the protein levels of RTN3 were significantly increased in hippocampi and cortices of DCTN6+/− mice compared to DCTN6+/+ mice (Figure 2A-B).

To examine whether increased RTN3 protein levels in DCTN6-deficient mice also enhance dispersed RIDN formation during aging, the brain sections from 7- and 12-month-old DCTN6+/+ and DCTN6+/− mice were stained with tubular ER-associated RIDN markers (including RTN3, REEP2, and REEP5) (supplemental Figure 3). RIDNs were not detected in 6-month-old WT mouse brains, but were found in the hippocampal CA1 region at 12 months old, consistent with an increase in older mouse brains (Sharoar et al., 2016; Shi et al., 2009). The tubular ER-shaping proteins, RTN3, REEP2 (supplemental Figure 3), and REEP5 (data not shown) barely marked RIDNs when we stained 7-month-old DCTN6+/+ mouse brains. However, a few RIDNs were marked by RTN3 and REEP2 antibodies in the hippocampal CA1 area of DCTN6+/− mice at this age (indicated by white arrowheads in supplemental Figure 3, upper right panel). In 12-month-old DCTN6+/+ mouse CA1 regions, RTN3 and REEP2 colocalized RIDNs were clearly visible, however the number of RIDNs was increased in DCTN6+/− mouse brains (Figure 2C and supplemental Figure 3). We confirmed these results by staining several brain sections obtained from a pair of DCTN6+/− 12-month-old mice and their two DCTN6+/+ littermates and quantified the number of RIDNs on every 10 th section among 70 serial sections. Our quantification results showed a significant increase in RIDN numbers in DCTN6+/− mouse brains compared to their DCTN6+/+ littermates (Figure 2D).

Reduced DCTN6 expression enhances RTN3 aggregation and RIDN formation in Tg-RTN3 mouse brains

In Tg-RTN3 mouse brains, RTN3 protein level is increased 4-fold and HMW-RTN3 aggregates are significantly enhanced in the hippocampal area; the degree of RTN3 aggregation correlates with the formation of RIDNs in these mice (Hu et al., 2007). To investigate the effects of DCTN6 deficiency on RTN3 aggregation and RIDN formation in this mouse model, we created DCTN6-deficient Tg-RTN3 (Tg-RTN3;DCTN6$^{+/-}$) mice and compared with their WT Tg-RTN3 (Tg-RTN3;DCTN6$^{+/+}$) littermates. A comparison of endogenous (En)-RTN3, transgenic or exogenous (Ex)-RTN3, and HMW-RTN3 protein

Author Manuscript Author Manuscript Author Manuscript Author Manuscript

levels between 6-month-old Tg-RTN3;DCTN6$^{+/+}$ and Tg-RTN3;DCTN6$^{+/-}$ mice showed a significant enhancement of En-RTN3 levels in Tg-RTN3;DCTN6$^{+/-}$ cortices compared to their Tg-RTN3;DCTN6$^{+/+}$ littermates (Figure 3A-B). However, the protein levels of all RTN3 species were significantly increased in hippocampi of Tg-RTN3;DCTN6$^{+/-}$ mice compared to Tg-RTN3;DCTN6$^{+/+}$ mice, with a prominent increase of En-RTN3 protein levels in DCTN6-deficient Tg-RTN3 mice. We did not notice any significant alteration in REEP2 protein level in DCTN6-deficient Tg-RTN3 mice.

To compare RIDN formation in Tg-RTN3;DCTN6$^{+/+}$ and Tg-RTN3;DCTN6$^{+/-}$ mice hippocampi, we stained brain sections with RTN3- and REEP2-specific antibodies (Figure 3C). RTN3- and REEP2-colocalized RIDNs were increased in Tg-RTN3;DCTN6$^{+/-}$ mouse brains compared to their Tg-RTN3;DCTN6$^{+/+}$ littermates. To make a quantifiable comparison of RIDN formation, the numbers of RIDNs in the hippocampus area on every 10th section among 70 serial sections obtained from one-half of the brains (the other halves were used for western blot analysis) from Tg-RTN3;DCTN6$^{+/+}$ and Tg-RTN3;DCTN6$^{+/-}$ mice were quantified after threshold adjustment using ImageJ (Fiji) software (an example shown in supplemental Figure 4a-b). We counted an average of 1037±86.27 RIDNs in 7 sections from each Tg-RTN3;DCTN6$^{+/+}$ mouse (n=2) and this number was significantly increased to 1391±65.05 RIDNs in Tg-RTN3;DCTN6$^{+/-}$ mice (n=2) (Fig. 3D). Altogether, these results indicated an influential effect of DCTN6 deficiency on hippocampus-specific RTN3 aggregation and on disperse RIDN formation in WT and Tg-RTN3 mouse brains.

Enhanced accumulation of axonal RTN3 in DCTN6-deficient neurons

DCTN6 plays critical roles in dynein-mediated retrograde axonal transport (Yeh et al., 2012). Our co-IP study showed that DCTN6 specifically interacts with the N-terminal domain of RTN3. To determine whether enhanced RIDN formation in DCTN6-deficient mouse brains is a consequence of RTN3 accumulation in axons due to impaired retrograde trafficking, we cultured primary neurons from DCTN6+/+ and DCTN6+/− mouse embryos and investigated the RTN3 staining pattern in neurites. A reduced DCTN6 antibody staining was noticeable in DCTN6+/− neurons compared to DCTN6+/+ neurons (supplemental Figure 5a-b). Although, colocalization of RTN3 and DCTN6 was observed in neuronal soma and neurites in both DCTN6+/+ and DCTN6+/− neurons, a beads-on-a-string morphology of RTN3 aggregates was more apparent in the neurites of DCTN6+/− neurons (supplemental Figure 5b, right-bottom panel). To investigate whether those RTN3 aggregates accumulate in axons, we co-stained primary cultured neurons with RTN3 and MAP2 antibodies (Figure 4A-D). The dendrite marker MAP2 labeled most of the neurites of a neuron except a probable axon that protruded from same neuronal soma (indicated by white arrowhead in Figure 4C-D). RTN3-aggregated puncta were visible in a beads-on-a-string morphology along axons with a prominent appearance in DCTN6+/− neurons compared to DCTN6+/+ neurons (indicated by green arrowhead in Figure 4C-D). We also observed many other beads-on-a-string that were not stained by MAP2 antibody, but their attachment with neuronal soma was not traceable (drawn by white dotted lined in Figure 4E-F). We have quantified the number of beads that were traceable on a string in several randomly obtained pictures from DCTN6+/+ and DCTN6+/− neurons. Our quantification showed a significant enhancement of axonal bead morphology of RTN3 staining in DCTN6+/−

Author Manuscript Author Manuscript Author Manuscript Author Manuscript

neurons compared to DCTN6+/+ neurons (Figure 4G). This evidence suggested an enhanced accumulation of RTN3 aggregates in swelled axons in DCTN6-deficient neurons, likely due to impaired retrograde trafficking of RTN3 by dynein-dynactin motors.

Minimal impacts of AAV-mediated DCTN6 overexpression on RIDN formation

Our results showed that DCTN6 protein level is reduced in the hippocampus, and DCTN6 deficiency enhances the formation of hippocampus-specific dispersed RIDNs in WT and Tg-RTN3 mouse brains (Figures 2 and 3). To investigate whether the enhancement of DCTN6 expression can reduce RIDN formation, we co-expressed DCTN6 with RTN3 in the hippocampal area of WT mice and observed its effects on RIDN formation. RTN3 was overexpressed with the synapsin promoter through AAV-mediated delivery (AAV-*syn*-RTN3) in the hippocampus area of 2-month-old WT mice. The overexpression of RTN3 in the injected area of the hippocampus was confirmed by enhanced RTN3 signal when the fixed brain sections were stained with RTN3 antibody after 2 weeks of AAV injection, *i.e.*, post-injection day (PID)-15 (Figure 5A and supplemental Figure 6a). At PID-21, we observed a sparse number of swelled neurites—likely the initiation of RIDN formation—in RTN3-expressing neurons in a granular layer at the injection site (indicated in white dotted box in Figure 5B, magnified views shown in the inset). At PID-60, a clear RIDN morphology was visible within the injected area, and the number and size of RIDNs were increased at PID-120 (Figure 5C-D and supplemental Figure 6bc).

Next, we co-injected AAV-syn-RTN3 and AAV-syn-DCTN6eGFP or AAV-syn-eGFP (as a control) into the hippocampal area (supplemental Figure 6d). Similar to our observation in AAVsyn-RTN3 injected mice, we noticed an initiation of RIDN formation in AAV-syn-RTN3 and AAV-syn-eGFP co-injected mouse brains at PID-21 (indicated in white dotted box in Figure 5E, magnified views shown in the inset). However, such morphology was rarely observed at the injected area of AAV-syn-RTN3 and AAV-syn-DCTN6eGFP co-injected mouse brains (Figure 5F). To determine whether DCTN6 overexpression could reduce the amount of RIDNs, we stained the brain sections of AAV-syn-RTN3; AAV-syn-eGFP and AAV-syn-RTN3; AAV-synDCTN6eGFP-injected mice after 4 months of injection and quantified RIDNs at the injected areas on every 10^{th} section among ~60 serial sections. We observed no significant differences in the numbers of RIDN between AAV-syn-eGFP and AAV-syn-DCTN6eGFP-injected injected mice (Figure 5G-H, supplemental Figure 6e). To further examine the effects of DCTN6 overexpression on endogenous RTN3 protein levels, we also transfected AAV-syn-eGFP and AAV-syn-DCTN6eGFP into primary cultured neurons from E17 WT mice (supplemental Figure 7a) and performed Western blot analysis to measure RTN3 and REEP2 protein levels (supplemental Figure 7b). We also observed no significant alteration in RTN3 and REEP2 protein levels when DCTN6 was overexpressed (supplemental Figure 7c). These results indicated that exogenous overexpression of DCTN6 does not reduce RIDNs. This could be due to inefficient complex formation by exogenous DCTN6 with DCTN5 and other components of DCTN.

Author Manuscript Author Manuscript Author Manuscript Author Manuscript

Discussion

The formation of DNs is a distinguishing feature of AD brains because a diffused form of Aβ plaques is also present in cognitively normal elder human brains that lack DNs (Dickson et al., 1999; Fukumoto et al., 1996; Joachim et al., 1989; Lenders et al., 1989). RIDNs comprise a major proportion of DNs in AD brains compared to other types of DNs that are detected by tau, ubiquitin, or neurofilaments (Dickson et al., 1999; Hu et al., 2007; Lenders et al., 1989). Hippocampus-specific disperse RIDN formation is a spontaneous process during aging in mouse brains, and an acceleration of such aging-associated RIDN formation in Tg-RTN3 mouse brains impairs synaptic function in those mice (Hu et al., 2007; Sharoar et al., 2016; Shi et al., 2009). Tubular ER are abnormally accumulated in both clustered and dispersed types of RIDNs, and RTN3 likely has an active role for such tubular ER clustering in RIDNs because RIDNs cannot be marked by other tubular ER markers such as REEP2 and REEP5 in RTN3-deficient aged mouse brains (Sharoar et al., 2016).

As the largest cellular organelle, the ER is thoroughly distributed from neuronal soma to distant neurites with a predominant localization of tubular ER domain in axons and dendrites (Farías et al., 2019; Öztürk et al., 2020; Tsukita and Ishikawa, 1976; Yalçın et al., 2017). ER tubules dynamically traffic in axons by microtubule-based kinesin-1 or KIF5 and dynein motors in anterograde and retrograde directions, respectively (De Vos and Hafezparast, 2017; Farías et al., 2019). The dynein-powered trafficking needs the dynactin complex for its activation and binding with cargo membranes (Cianfrocco et al., 2015; Schroer, 2004). Two dynactin subunits, DCTN5 and DCTN6, also known as p25 and p27, respectively, are localized at the dynactin pointed-end complex and are involved in membrane binding during endosomal trafficking and mitotic-spindle arrangement (Schroer, 2004; Yeh et al., 2012). Hence, a specific interaction between RTN3 and DCTN6 is likely functionally involved in retrograde transport of ER tubules from axonal termini to neuronal soma.

RTNs and REEPs are members of two major protein families that are involved in membrane tubulation of the smooth ER domain (Goyal and Blackstone, 2013; Hu et al., 2008; Hu et al., 2009). All these ER tubule-shaping proteins dictate ω-shape membrane topology, in which two transmembrane domains are attached to the membrane and both C- and N-terminal domains protrude into the cytosol (Goyal and Blackstone, 2013; He et al., 2007). Interactions of hydrophobic transmembrane domains of tubular ER-shaping proteins are involved in membrane curvature, tubule formation, and extension of tubular networks (Bjork et al., 2013; Goyal and Blackstone, 2013; Hu et al., 2008; Park et al., 2010; Voeltz et al., 2006). A specific interaction of DCTN6 with the N-terminal cytosolic domain of RTN3 suggests that in addition to ER tubule shaping, RTN3 plays critical roles in tubular ER trafficking, maintaining axonal ER dynamics, and ER tubule distribution (Farías et al., 2019; Öztürk et al., 2020). A reduced DCTN6 protein level may cause functional deficiency of ER trafficking in axons, which could imbalance ER distribution and increase the accumulation of RTN3 at the axonal boutons (Figure 4 and supplemental Figure 2). Enhanced curvature of tubular ER likely occurs at such RTN3-enriched areas that induce RTN3-REEP inclusion formation, which ultimately leads to RIDN formation and mitochondria degeneration at ER tubule-accumulated areas (Sharoar et al., 2016).

Author Manuscript Author Manuscript Author Manuscript Author Manuscript

RTN3 protein levels increase during aging in WT mouse brains (Shi et al., 2009), and RTN3 undergoes spontaneous aggregation to form HMW-RTN3; the degree of RTN3 aggregation corresponds to both clustered and disperse RIDN formation in AD and Tg-RTN3 mouse brains (Hu et al., 2007). Here we demonstrate that RTN3 protein levels are increased and the formation of hippocampus-specific disperse RIDNs is enhanced in DCTN6-deficient mouse brains (Figure 2, supplemental Figure 3). In DCTN6-deficient Tg-RTN3 mouse brains, the levels of HMW-RTN3, Ex-RTN3, and En-RTN3 proteins and tubular ER-associated RIDN formation were significantly increased compared to DCTN6+/+;Tg-RTN3 mouse brains (Figure 3). The impact of DCTN6 deficiency on En-RTN3 protein levels was prominent compared to Ex-RTN3 levels in Tg-RTN3 mouse brains (Figure 3A-B). This could be due to preferential binding between mouse DCTN6 and the N-terminal domains of endogenous RTN3 since N-terminal sequence of human RTN3 (transgene) differs from that of mouse RTN3 by about 20% (data not shown). Additionally, it is possible that an artificial several-fold increase of RTN3 expression may catalyze and enhance intermolecular interaction and aggregation of RTN3 that readily induces RTN3-REEP-enriched tubular ER accumulation in RIDNs at axonal termini (Hu et al., 2007; Sharoar et al., 2016). DCTN6 deficiency probably aggravates these processes due to impairment of DCTN6-RTN3-mediated tubular ER trafficking (Figure 4), and it may also increase the contribution of endogenous RTN3 to RIDN formation (Figure 2C-D).

DCTN6 and DCTN5 form a heterodimer, and they stabilize one another (Yeh et al., 2012). Therefore, we were not surprised that we observed a reduction of DCTN5 protein levels in DCTN6-deficient mouse brains (Figure 2A-B). Both DCTN6 and DCTN5 protein levels were reduced in the hippocampus during aging in WT mice (supplemental Figure 2b-d). Hence, an impaired function in tubular ER retrograde trafficking due to reduced DCTN5/DCTN6 (p25/p27) heterodimer functions may contribute to increased RTN3 levels (Figures 2A-B and 3A-B) and progressive RIDN formation during aging (Figures 2C-D and 3C-D) (Sharoar et al., 2016; Shi et al., 2009; Yeh et al., 2012). In yeast, it has been shown that DCTN5 is critical for endosome binding, while the function of DCTN6 is dispensable in this process (Qiu et al., 2018). It is possible that reduced DCTN5 may also increase tubular ER-accumulated RIDNs due to functional deficiency of p25/p27 as an integrated unit in a pointed-end complex (Yeh et al., 2012). However, our yeast two-hybrid study did not identify any sequences that match DCTN5 (supplemental Table 1); but, DCTN5, ARP11, and DCTN4 were co-IPed with RTN3 in Tg-RTN3 mouse brains (data not shown), which is likely due to the participation of these proteins including DCTN6 as an integrated structure of the pointed-end complex of dynactin (Schroer, 2004; Yeh et al., 2012). A specific interaction of DCTN6 with the cytosolic RTN3 N-terminal domain (Figure 1D) strongly suggests that DCTN6 is a key component of the dynactin pointed-end complex, which likely mediates tubular ER trafficking. However, an inefficient inhibitory effect on RTN3 protein level and RIDN formation by AAV-mediated overexpression of DCTN6 alone (Figure 5 and supplemental Figure 6e) suggests that exogenous enhancement of DCTN6 may not efficiently form a complex with other components of DCTN to enhance function. Instead, an excessive expression of DCTN6 may have negative impact on complex formation and its function (Burkhardt et al., 1997; Quintyne et al., 1999). This suggests that a balance among protein levels of different sub-units may be necessary for structural integrity

Author Manuscript Author Manuscript Author Manuscript Author Manuscript

of the DCTN complex and its function in axonal transport and organelle distribution. A decrease of DCTN6/DCTN5 and an increase of DCTN4 protein levels during aging (supplemental Figure 2b-c) may change the equilibrium, which eventually may impair the dynein-dynactin functions to transport tubular ER from axonal termini to neuronal soma. Further investigation may elucidate the underlaying mechanisms of this process.

To conclude, our study elucidated a novel DCTN6-RTN3 interaction that likely functions in tubular ER trafficking and its distribution in axons. An impairment in DCTN6-RTN3-mediated tubular ER trafficking due to DCTN6 deficiency during aging is a contributing factor to tubular ER-accumulated RIDN formation, mitochondria degeneration, and cognitive deficits during aging (Hu et al., 2007; Sharoar et al., 2016; Shi et al., 2009). We propose that preserving DCTN6-mediated tubular ER distribution in neurons may improve cognition in the aging population.

Supplementary Material

Refer to Web version on PubMed Central for supplementary material.

Acknowledgements

We thank Dr. Christopher Bonin and Dr. Geneva Hargis for critical reading of this manuscript. This work is supported by an award from Alzheimer's Association to (AARF-17-504724) MGS and NIH grants to RY (AG025493 and RFA046929).

References

Bjork S, Hurt CM, Ho VK, Angelotti T, 2013. REEPs are membrane shaping adapter proteins that modulate specific g protein-coupled receptor trafficking by affecting ER cargo capacity. PLoS One 8(10), e76366. [PubMed: 24098485]

Burkhardt JK, Echeverri CJ, Nilsson T, Vallee RB, 1997. Overexpression of the dynamitin (p50) subunit of the dynactin complex disrupts dynein-dependent maintenance of membrane organelle distribution. J Cell Biol 139(2), 469–484. [PubMed: 9334349]

Cianfrocco MA, DeSantis ME, Leschziner AE, Reck-Peterson SL, 2015. Mechanism and regulation of cytoplasmic dynein. Annu Rev Cell Dev Biol 31, 83–108. [PubMed: 26436706]

De Vos KJ, Hafezparast M, 2017. Neurobiology of axonal transport defects in motor neuron diseases: Opportunities for translational research? Neurobiol Dis 105, 283–299. [PubMed: 28235672]

Dickson TC, King CE, McCormack GH, Vickers JC, 1999. Neurochemical diversity of dystrophic neurites in the early and late stages of Alzheimer's disease. Exp Neurol 156(1), 100–110. [PubMed: 10192781]

Farías GG, Fréal A, Tortosa E, Stucchi R, Pan X, Portegies S, Will L, Altelaar M, Hoogenraad CC, 2019. Feedback-Driven Mechanisms between Microtubules and the Endoplasmic Reticulum Instruct Neuronal Polarity. Neuron 102(1), 184–201.e188. [PubMed: 30772082]

Fukumoto H, Asami-Odaka A, Suzuki N, Shimada H, Ihara Y, Iwatsubo T, 1996.

Amyloid beta protein deposition in normal aging has the same characteristics as that in Alzheimer's disease. Predominance of A beta 42(43) and association of A beta 40 with cored plaques. Am J Pathol 148(1), 259–265. [PubMed: 8546214]

Goyal U, Blackstone C, 2013. Untangling the web: mechanisms underlying ER network formation. Biochim Biophys Acta 1833(11), 2492–2498. [PubMed: 23602970]

He W, Hu X, Shi Q, Zhou X, Lu Y, Fisher C, Yan R, 2006. Mapping of interaction domains mediating binding between BACE1 and RTN/Nogo proteins. J Mol Biol 363(3), 625–634. [PubMed: 16979658]

Author Manuscript Author Manuscript Author Manuscript Author Manuscript

He W, Shi Q, Hu X, Yan R, 2007. The membrane topology of RTN3 and its effect on binding of RTN3 to BACE1. J Biol Chem 282(40), 29144–29151. [PubMed: 17699523]

Hu J, Shibata Y, Voss C, Shemesh T, Li Z, Coughlin M, Kozlov MM, Rapoport TA, Prinz WA, 2008. Membrane proteins of the endoplasmic reticulum induce high-curvature tubules. Science 319(5867), 1247–1250. [PubMed: 18309084]

Hu J, Shibata Y, Zhu PP, Voss C, Rismanchi N, Prinz WA, Rapoport TA, Blackstone C, 2009. A class of dynamin-like GTPases involved in the generation of the tubular ER network. Cell 138(3), 549–561. [PubMed: 19665976]

Hu X, Shi Q, Zhou X, He W, Yi H, Yin X, Gearing M, Levey A, Yan R, 2007. Transgenic mice overexpressing reticulon 3 develop neuritic abnormalities. EMBO J 26(11), 2755–2767. [PubMed: 17476306]

Joachim CL, Morris JH, Selkoe DJ, 1989. Diffuse senile plaques occur commonly in the cerebellum in Alzheimer's disease. Am J Pathol 135(2), 309–319. [PubMed: 2675616]

Lenders MB, Peers MC, Tramu G, Delacourte A, Defossez A, Petit H, Mazzuca M, 1989. Dystrophic neuropeptidergic neurites in senile plaques of Alzheimer's disease precede formation of paired helical filaments. Acta Neurol Belg 89(3–4), 279–285. [PubMed: 2516978]

Nixon RA, Wegiel J, Kumar A, Yu WH, Peterhoff C, Cataldo A, Cuervo AM, 2005. Extensive involvement of autophagy in Alzheimer disease: an immuno-electron microscopy study. J Neuropathol Exp Neurol 64(2), 113–122. [PubMed: 15751225]

Oertle T, Schwab ME, 2003. Nogo and its paRTNers. Trends Cell Biol 13(4), 187–194. [PubMed: 12667756]

Öztürk Z, O'Kane CJ, Pérez-Moreno JJ, 2020. Axonal Endoplasmic Reticulum Dynamics and Its Roles in Neurodegeneration. Front Neurosci 14, 48. [PubMed: 32116502]

Park SH, Zhu PP, Parker RL, Blackstone C, 2010. Hereditary spastic paraplegia proteins REEP1, spastin, and atlastin-1 coordinate microtubule interactions with the tubular ER network. J Clin Invest 120(4), 1097–1110. [PubMed: 20200447]

Prior M, Shi Q, Hu X, He W, Levey A, Yan R, 2010. RTN/Nogo in forming Alzheimer's neuritic plaques. Neurosci Biobehav Rev 34(8), 1201–1206. [PubMed: 20144652]

Qiu R, Zhang J, Xiang X, 2018. p25 of the dynactin complex plays a dual role in cargo binding and dynactin regulation. J Biol Chem 293(40), 15606–15619. [PubMed: 30143531]

Quintyne NJ, Gill SR, Eckley DM, Crego CL, Compton DA, Schroer TA, 1999. Dynactin is required for microtubule anchoring at centrosomes. J Cell Biol 147(2), 321–334. [PubMed: 10525538]

Schindelin J, Arganda-Carreras I, Frise E, Kaynig V, Longair M, Pietzsch T, Preibisch S, Rueden C, Saalfeld S, Schmid B, Tinevez JY, White DJ, Hartenstein V, Eliceiri K, Tomancak P, Cardona A, 2012. Fiji: an open-source platform for biological-image analysis. Nat Methods 9(7), 676–682. [PubMed: 22743772]

Schroer TA, 2004. Dynactin. Annu Rev Cell Dev Biol 20, 759–779. [PubMed: 15473859]

Sharoar MG, Hu X, Ma XM, Zhu X, Yan R, 2019. Sequential formation of different layers of dystrophic neurites in Alzheimer's brains. Mol Psychiatry.

Sharoar MG, Shi Q, Ge Y, He W, Hu X, Perry G, Zhu X, Yan R, 2016. Dysfunctional tubular endoplasmic reticulum constitutes a pathological feature of Alzheimer's disease. Mol Psychiatry 21(9), 1263–1271. [PubMed: 26619807]

Sharoar MG, Yan R, 2017. Effects of altered RTN3 expression on BACE1 activity and Alzheimer's neuritic plaques. Rev Neurosci 28(2), 145–154. [PubMed: 27883331]

Shi Q, Ge Y, He W, Hu X, Yan R, 2017. RTN1 and RTN3 protein are differentially associated with senile plaques in Alzheimer's brains. Sci Rep 7(1), 6145. [PubMed: 28733667]

Shi Q, Hu X, Prior M, Yan R, 2009. The occurrence of aging-dependent reticulon 3 immunoreactive dystrophic neurites decreases cognitive function. J Neurosci 29(16), 5108–5115. [PubMed: 19386906]

Shi Q, Prior M, Zhou X, Tang X, He W, Hu X, Yan R, 2013. Preventing formation of reticulon 3 immunoreactive dystrophic neurites improves cognitive function in mice. J Neurosci 33(7), 3059–3066. [PubMed: 23407961]

Author Manuscript Author Manuscript Author Manuscript Author Manuscript

Shibata Y, Voss C, Rist JM, Hu J, Rapoport TA, Prinz WA, Voeltz GK, 2008. The reticulon and DP1/Yop1p proteins form immobile oligomers in the tubular endoplasmic reticulum. J Biol Chem 283(27), 18892–18904. [PubMed: 18442980]

Tsukita S, Ishikawa H, 1976. Three-dimensional distribution of smooth endoplasmic reticulum in myelinated axons. J Electron Microsc (Tokyo) 25(3), 141–149. [PubMed: 1025229]

Voeltz GK, Prinz WA, Shibata Y, Rist JM, Rapoport TA, 2006. A class of membrane proteins shaping the tubular endoplasmic reticulum. Cell 124(3), 573–586. [PubMed: 16469703]

Yalçın B, Zhao L, Stofanko M, O'Sullivan NC, Kang ZH, Roost A, Thomas MR, Zaessinger S, Blard O, Patto AL, Sohail A, Baena V, Terasaki M, O'Kane CJ, 2017. Modeling of axonal endoplasmic reticulum network by spastic paraplegia proteins. Elife 6.

Yeh TY, Quintyne NJ, Scipioni BR, Eckley DM, Schroer TA, 2012. Dynactin's pointed-end complex is a cargo-targeting module. Mol Biol Cell 23(19), 3827–3837. [PubMed: 22918948]

Author Manuscript Author Manuscript Author Manuscript Author Manuscript

Highlights

1. The N-terminal domain of reticulon 3 (RTN3) interacts with dynactin 6 (DCTN6).
2. RTN3-DCTN6 interaction likely mediates the tubular ER transport in axons.
3. DCTN6 deficiency increases protein levels and aggregation of RTN3.
4. Reduced DCTN6 during aging contributes to $RTN3^{+}$ dystrophic neurite formation.

Author Manuscript Author Manuscript Author Manuscript Author Manuscript

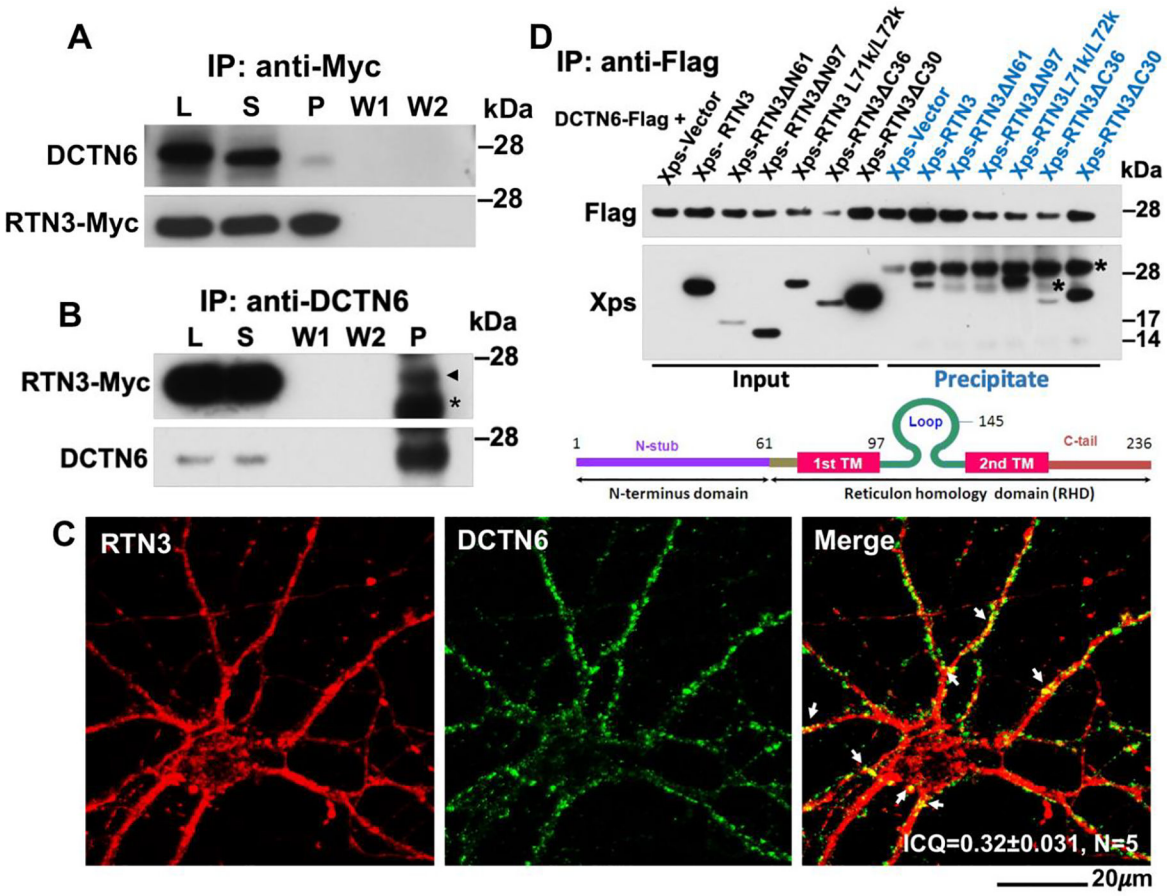

Figure 1. DCTN6 interacts with the N-terminal domain of RTN3 in neurons.

Myc-tagged RTN3 (**A**) or endogenous DCTN6 (**B**) was immunoprecipitated (IP) with anti-Myc beads or a DCTN6 antibody, respectively, from Tg-RTN3 mouse brain lysate. The input or lysate (L), supernatant (S), precipitate (P), 1st wash (W1), and 2nd wash (W2) were subjected to Western blot analysis with DCTN6 and RTN3 antibodies. DCTN6 was co-IPed with Myc-RTN3 and RTN3 (indicated by arrowhead) was precipitated with DCTN6. Primary cultured hippocampal neurons from E17 WT mice were stained with RTN3- and DCTN6-specific antibodies (**C**). Some RTN3 and DCTN6 colocalized puncta are indicated by the white arrows. ICQ correlation coefficient value was calculated using Fiji (ImageJ) software. Scale bar shown at the bottom. <>HEK293 cells were co-transfected with various Xpress (Xsp)-tagged RTN3 domain deletion mutants and Flag-tagged DCTN6 (DCTN6-Flag), the lysates from transfected cells were used for IP with anti-Flag beads, and input and precipitate were subjected to Western blot analysis using anti-Flag and anti-Xpress antibodies (**D**). The names of each construct are depicted by the deleted numbers of residues from either the N- or C-terminal end of RTN3. Domains in RTN3 and relative positions in the deletion constructs are illustrated in the diagrams. Empty vector construct was co-expressed as a control. RTN3 was not co-IPed when N-terminal 1–61 (RTN3ΔN61) or 1–91 (RTN3ΔN91) amino acids were deleted. Nonspecific bands are indicated by asterisks.

Author Manuscript Author Manuscript Author Manuscript Author Manuscript

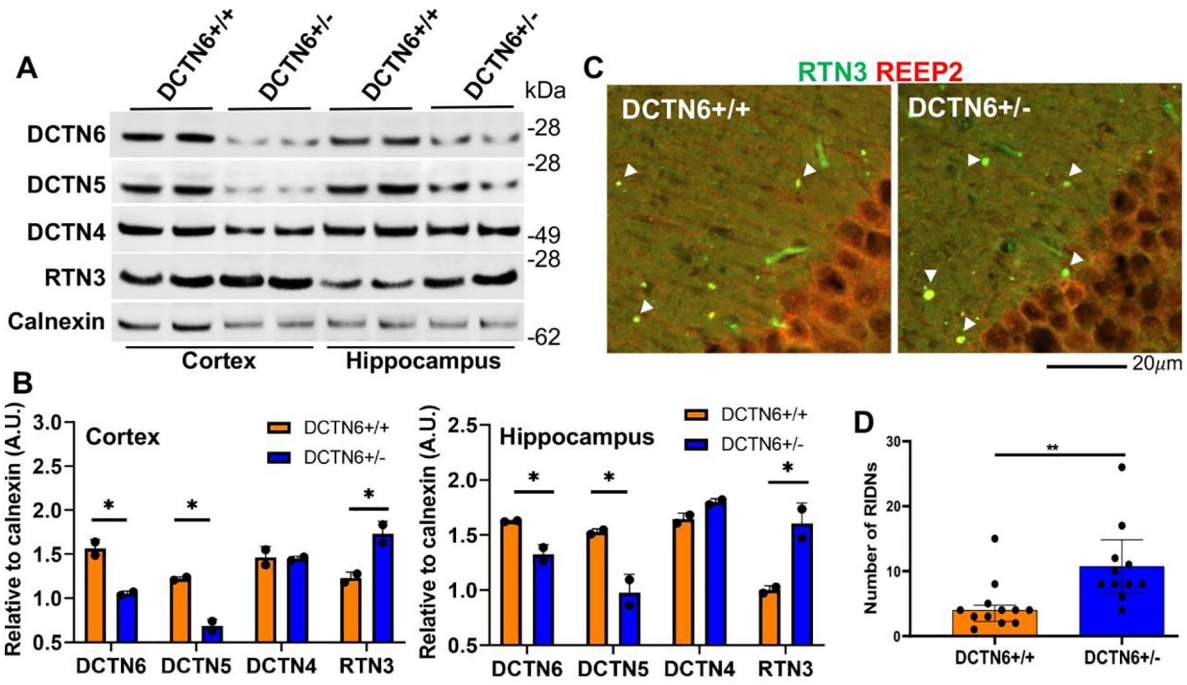

Figure 2. DCTN6 deficiency enhances RTN3 protein levels and RIDN formation in WT mouse brains.

The cortical and hippocampal lysates from DCTN6 heterozygotes (DCTN6+/−) and their WT littermates (DCTN6+/+) were subjected to Western blot analysis using DCTN6, DCTN5, DCTN4, RTN3, and calnexin antibodies (**A**). Band intensities (mean gray value in a fixed area) for each protein were measured by Fiji (ImageJ) software and the average of each group was calculated and standardized by dividing with the value for calnexin (**B**). A.U. indicates arbitrary units. The fixed brain sections from 12-month-old DCTN6+/+ or DCTN6+/− mice were stained with RTN3 and REEP2 antibodies (**C**). Some RIDNs are indicated by white arrowheads. Scale bar shown at the bottom. The numbers of RIDNs on every 10th section among 70 serial sections from half-brains from each group (two mice each group) were blindly quantified **(D)**. * and ** indicates significance at P<0.05 and P<0.01 (Student's T-test), respectively. Individual data points are displayed (•), and error bars represent standard deviation.

Author Manuscript Author Manuscript Author Manuscript Author Manuscript

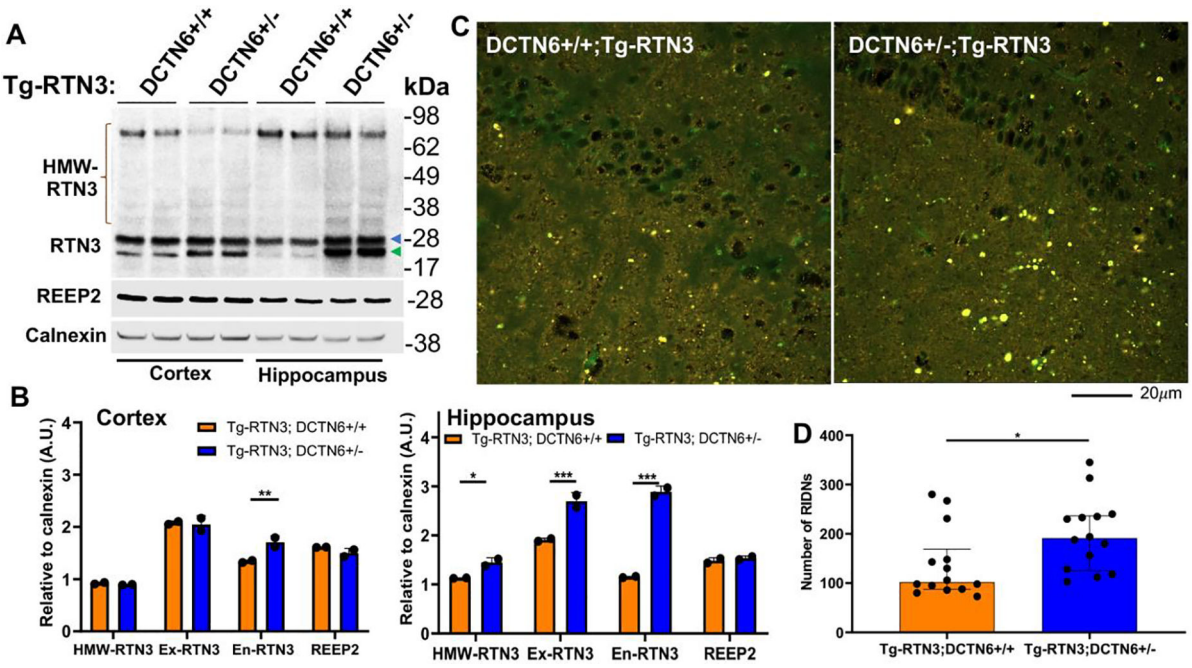

Figure 3. Enhanced RTN3 aggregation and RIDN formation in DCTN6-deficient Tg-RTN3 mouse brains.

The cortical and hippocampal lysates from DCTN6+/+ and DCTN6+/− Tg-RTN3 mice were subjected to Western blot analysis (**A**). The band intensity of different RTN3 species, such as RTN3 aggregates, demonstrated by high molecular weight RTN3 (HMW-RTN3, indicated by bracket in panel A), RTN3 transgene/exogenous RTN3 (Ex-RTN3, indicated by blue arrowhead in panel A), and endogenous RTN3 (En-RTN3, indicated by green arrowhead in panel A) were measured and standardized with the band intensity of calnexin for respective groups (**B**). Fixed brain sections from 6-month-old DCTN6+/+ or DCTN6+/− Tg-RTN3 mice were stained with RTN3 and REEP2 antibodies (**C**). Scale bar shown at the bottom. The numbers of RIDNs on every 10 sections for 70 serial sections from DCTN6+/+;Tg-RTN3 and DCTN6+/−;Tg-RTN3 mouse brains were quantified and the sum of RIDNs for 7 sections in each mouse (two mice per group) was calculated and compared (**D**). A.U. indicates arbitrary units. *, **, and *** indicates significance at P<0.05, P<0.01, and P<0.001 (Student's T-test), respectively. Individual data points are displayed (•), and error bars represent standard deviation.

Author Manuscript Author Manuscript Author Manuscript Author Manuscript

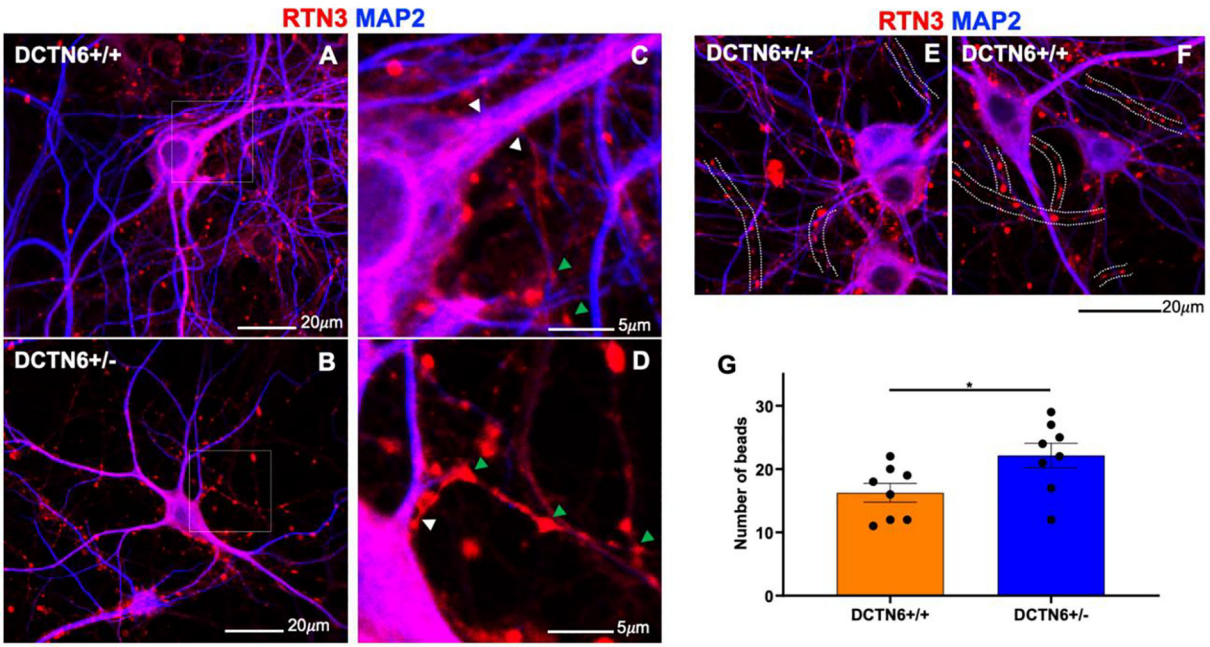

Figure 4.

Primary hippocampal neurons were cultured from E17 DCTN6+/+ and DCTN6+/− mice and co-stained with RTN3 and MAP2 antibodies (A-F). The areas in white dotted boxes in **A** and **B** are enlarged in **C** and **D**, respectively. The origin of axons from neuronal soma are indicated by white arrowheads. The beads-on-string morphology within axons are indicated by green arrowheads. Scale bar shown in each panel. A few beads-on-a-string are traced and marked by white dotted lines (E and F). Scale bar shown at the bottom. The beads on traceable strings in randomly obtained pictures from DCTN6+/+ and DCTN6+/− neurons were quantified **(G)**. * indicates P<0.05 (Student's T-test, N=8). Individual data points are displayed (•), and error bars represent standard deviation.

Author Manuscript Author Manuscript Author Manuscript Author Manuscript

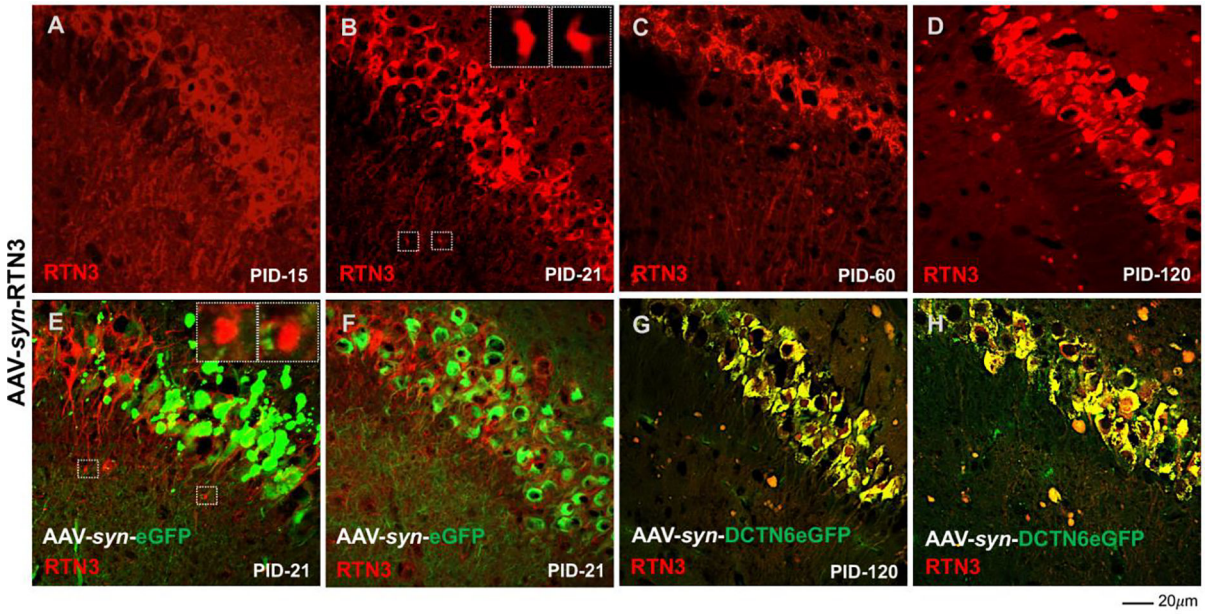

Figure 5. AAV-mediated DCTN6 co-expression minimally suppresses RTN3-overexpressed RIDN formation in WT mouse brain.

AAV-*syn*-RTN3 viral particles were injected into the hippocampal area of WT mouse brains; the brain samples were collected at post-injection day (PID)-15, 21, 60, and 120; and the fixed brain sections were stained with RTN3 antibody **(A-D)**. The initiation of RIDN formation that appeared as swelled neurites at PID-21 are indicated in dotted boxes and the magnified views are shown as insets in the panel (**B**). RIDNs number and size were consistently increased at PID-60 (**C**) and PID 120 (**D**). AAV-*syn*-RTN3 were co-injected either with AAV-syn-eGFP (**E** and **G**) or with AAV-*syn*- DCTN6eGFP (**F** and **H**) in the hippocampal area, and the brain samples were collected at PID-21 (**E-F**) and PID-120 (**G-H**) for immuno-confocal microscopy using RTN3 and GFP antibodies. RIDN formation at PID-21 is shown in in the dotted boxes and the magnified views are shown as insets in the panel **(E)**. The initiation of RIDN formation was not notable at PID-21 **(F)**. No changes of RIDN formation were observed at PID-120 in the injected area when DCTN6 was co-expressed with RTN3 (**G-H**). Scale bar shown at the bottom.